Journal of
Materials Chemistry A

Materials for energy and sustainability

Accepted Manuscript

This article can be cited before page numbers have been issued, to do this please use: O. Shinnawy, S. A. Hejazi and K. Amini, *J. Mater. Chem. A*, 2026, DOI: 10.1039/D6TA03239G.

ROYAL SOCIETY OF CHEMISTRY

rsc.li/materials-a

View Article Online
DOI: 10.1039/D6TA03239G

Dual-Function Electrochemical Cell for Simultaneous Carbon Capture and Lithium Extraction from Saline Waters

Omer Shinnawy, Seyyed Arman Hejazi, Kiana Amini*

Department of Materials Engineering, The University of British Columbia, 6350 Stores Road, Vancouver, BC V6T 1Z4, Canada

* *Corresponding author. E-mail address: kiana.amini@ubc.ca*

Abstract

Effective utilization of saline waters as a large reservoir of both dissolved inorganic carbon (DIC) and lithium would simultaneously support carbon mitigation and secure critical mineral supply. Here, we report the first demonstration of a dual-function electrochemical system capable of coupling CO_2 capture and Li^+ extraction from saline waters. Using a pH-swing architecture with bismuth and $LiFePO_4$ electrodes, we achieve stable pH cycling between 8.1 and 4.7 in 2.1 mM DIC, while extracting lithium at concentrations down to 0.17 ppm Li^+ (seawater levels). Under impurity-free conditions, the system maintains 80% bismuth utilization and 50% lithium utilization, with attractive energetic costs of 128 kJ/mol CO_2 and 121 kJ/mol Li, comparable to state-of-the-art stand-alone electrochemical systems. By integrating Li^+ and CO_2 extraction using shared pumping, membrane, and reactor infrastructure, this system offers a compelling path toward co-production of critical materials and integrated CO_2 capture using a single seawater-processing platform.

Keywords:

Carbon capture, Lithium extraction, Electrochemical systems, Dual-function electrochemical cells, Saline waters, Seawater

Introduction

To meet climate targets, particularly the goal of limiting warming to 1.5 °C by 2050, carbon removal efforts must scale up to around 10 Gt per year [1]. While mitigation efforts have focused mainly on point-source and air-based capture systems, recent studies have highlighted the largely untapped potential of capturing CO_2 from surface waters [2–6]. The ocean is part of the global carbon cycle, meaning that when CO_2 is captured from seawater and the processed water is returned, it can reabsorb more CO_2 from the atmosphere, effectively making the ocean a renewable sink for CO_2. Oceans and other surface waters have already absorbed and stored a substantial share of anthropogenic CO_2. This existing uptake eliminates the need for an initial gas-phase capture step when targeting oceanic sources [2]. Moreover, CO_2 concentrations in seawater are much higher, about 100 mg/L compared to 0.77 mg/L in air, making extraction potentially more efficient [7]. The captured CO_2 can be injected into subsurface geological formations or reused as a feedstock for fuels and chemical synthesis.

In parallel, the rapid development of energy storage technologies and electronics has driven a sharp increase in global lithium demand, underscoring the need for more efficient and scalable lithium extraction methods. Approximately 27 million tons of lithium are contained in brines or salt lakes with concentrations between 30 and 1,000 ppm [8], while seawater holds an estimated 200 billion.

View Article Online
DOI: 10.1039/D6TA03239G

Conventional lithium extraction from brines, primarily via solar evaporation, is slow, typically requiring up to two years [9]. In contrast, electrochemical systems powered by renewable energy have recently demonstrated promising pathways for extracting lithium from both brine [10,11] and even seawater sources [12].

To date, electrochemical CO_2-capture and lithium-extraction technologies from saline waters have been developed exclusively as separate, stand-alone systems, even though both rely on the same seawater feedstocks. For example, in the majority of electrochemical cells reported for lithium extraction [10–16], lithium is intercalated into iron phosphate ($FePO_4$, FP) or manganese oxide (MnO_2, MO) electrodes on one half-cell, coupled with counter-reactions such as oxygen evolution on activated carbon or reduced graphene, or the Ag/AgCl redox reaction. These counter-reactions primarily function to close the circuit and enable electron flow. A similar design philosophy is seen in electrochemical systems for carbon capture from water resources. The basic operating principle of electrochemical CO_2 capture is to push the CO_2/bicarbonate equilibrium toward dissolved CO_2 by acidifying the seawater [17]. This acidification reaction has been coupled with the Ag/AgCl counter-reaction, primarily to mediate chloride ions [2], or bipolar membranes [18] have been used to create an acidified stream, with the ferrocyanide/ferricyanide redox couple driving ion movement and closing the circuit [5]. Acidification has also been achieved using oxygen and hydrogen evolution reactions [4,19,20].

The integration of CO_2 capture and lithium extraction within a single saline-water processing technology presents not only a dual solution to environmental and resource challenges but also a clear economic advantage. Both processes rely on water intake, pumping, and electrochemical infrastructure, allowing a combined system to maximize the utility of capital investment by producing two valuable outputs from related streams. By extracting lithium alongside carbon dioxide, the system enhances its commercial viability, diversifies its revenue streams, and increases its attractiveness to investors and policymakers seeking scalable solutions for climate mitigation and critical minerals supply.

In this work, we report the first proof-of-concept of a dual-function electrochemical cell capable of simultaneous carbon capture and lithium extraction. We first describe the working principles of the system, followed by a thermodynamic analysis to estimate its energy requirements. This is complemented by H-cell and flow-cell experiments, which demonstrate proof of concept and evaluate key performance metrics of the technology.

Working Principle

Fig. 1a illustrates the general principles of an electrochemical cell designed to perform both carbon capture and lithium extraction within a single system. The cell consists of an electrode capable of lithium intercalation, such as lithium iron phosphate (LFP), lithium manganese oxide (LMO), or similar intercalating materials on one side, and a proton-coupled electron transfer (PCET) electrode that acidifies the solution upon charging on the other side (Fig. 1b). It is preferable to use proton-coupled redox reactions where both the reaction and its products remain in solid forms, avoiding the introduction of new species to the water composition. Previous studies have reported the use of bismuth (Bi)/bismuth oxychloride (BiOCl) for seawater acidification [2]. Similarly, electrodes coated with anthraquinones [21] (rather than dissolved anthraquinones) are also promising candidates. The two sides are separated by an anion exchange membrane (AEM), which allows chloride ions (abundant in seawater) to carry the charge while preventing lithium leakage.

View Article Online
DOI: 10.1039/D6TA03239G

During the extraction and acidification step (Fig. 1a, left), lithium is extracted from seawater at the cathode, while the anode undergoes a PCET reaction (e.g., oxidation of bismuth), acidifying the solution. This acidification shifts the bicarbonate and carbonate equilibria toward dissolved CO_2, enabling CO_2 removal from seawater (Fig. S1). In the recovery and alkalization step (Fig. 1a, right), seawater is replaced with a recovery solution on the lithium side, and the intercalated lithium is released into this solution, creating a concentrated lithium stream. Meanwhile, at the BiOCl electrode, protons are consumed, causing the pH to rise. The processed water, with its pH adjusted, is then ready to be returned to ocean water to reabsorb CO_2.

The electrochemical system can be configured to use seawater on both sides or a combination of brine and seawater. Seawater typically contains less than 0.5 ppm lithium and has a pH of around 8.1 [22]. It can be circulated on both sides of the cell to achieve integrated lithium extraction and carbon capture. Alternatively, brine resources, such as desalination brine, are more concentrated in lithium and can be used on the lithium side for more efficient lithium extraction, while seawater is used on the carbon capture side. This configuration is particularly relevant for coastal desalination plants, where brine and seawater are both accessible and can be processed in parallel.

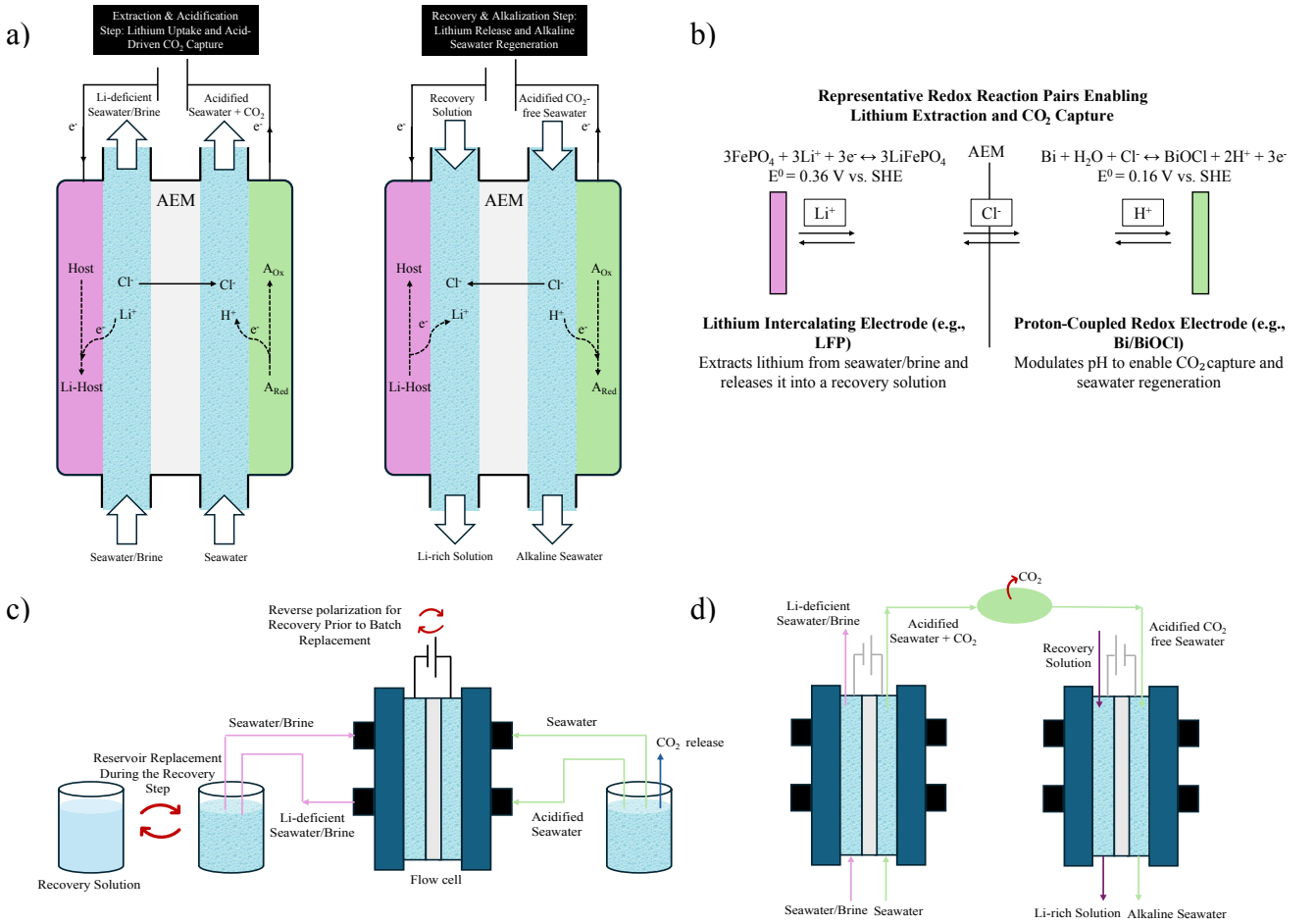

Fig. 1: Working principles of a dual-function electrochemical cell for simultaneous lithium extraction and carbon capture. (a) Schematic of the electrochemical cell during two operational steps: lithium uptake and proton-coupled electron transfer (PCET)-driven acidification for CO_2 capture (left), followed by lithium release and alkaline seawater regeneration (right). (b) Representative redox reaction pairs: lithium intercalation using $LiFePO_4$ and a solid-state PCET reaction using the Bi/BiOCl couple. (c) Batch operation mode. (d) Continuous operation mode using a dual-cell configuration with alternating flow and polarity switching.

View Article Online
DOI: 10.1039/D6TA03239G

The process can be operated in a single flow cell in batch mode (Fig. 1c), where a fixed volume of seawater is processed in discrete cycles, enabling controlled operation and decoupling of extraction and recovery steps. In the first step, seawater is circulated through the cell to enable lithium extraction and CO_2 capture. Once this step is complete, the seawater is replaced with a recovery solution on the lithium side only, while the PCET side (e.g., bismuth) remains unchanged. The cell polarity is then reversed to recover lithium into the recovery stream and regenerate alkaline seawater. Alternatively, the system can be designed as a continuous flow setup (Fig. 1d), which is more relevant for scalable operation, while the fundamental operating principle remains the same. In continuous mode, two cells operate in tandem until the electrodes reach depletion. At that point, the polarity and flow direction are switched (Fig. 1d).

Thermodynamic Analysis

To quantify the thermodynamic energetic cost in our dual-function electrochemical cell, we performed a thermodynamic analysis of a representative system (details in Supplementary information (SI) Section 1), focusing on the charge-balance-driven coupling between lithium intercalation and DIC conversion, considering Na^+ and Cl^- as the dominant ions governing solution salinity. Briefly, during the extraction and acidification step, the redox reactions are:

Positive electrode: $3FePO_4 + 3e^- + 3Li^+ \rightleftharpoons 3LiFePO_4 \qquad E^0 = 0.36\,V\ vs.\ SHE$ *(1)*

Negative electrode : $Bi + Cl^- + H_2O \rightleftharpoons BiOCl + 2H^+ + 3e^- \qquad E^0 = 0.16\,V\ vs.\ SHE$ *(2)*

Overall: $Bi + Cl^- + 3FePO_4 + 3Li^+ + H_2O \rightleftharpoons BiOCl + 3LiFePO_4 + 2H^+ \quad \Delta E^0 = 0.20\,V$ *(3)*

Based on these reactions, the thermodynamic cell voltage is:

$$\Delta E = \Delta E^o - \frac{R * T}{n * F} \ln \left(\frac{(\gamma_{H^+} * [H^+])^2}{\gamma_{Cl^-} * [Cl^-] * (\gamma_{Li^+} * [Li^+])^3} \right) \quad (4)$$

Where $[x]$ and γ_x are the concentration and activity coefficient of the compound x, respectively. Unlike the system coupling Bi/BiOCl with Ag/AgCl [2], where only proton and chloride activities influence the voltage, our system's cell voltage also depends on lithium concentration. As lithium is extracted and chloride ions migrate through the AEM during the extraction and acidification step, concentrations evolve according to:

$$[Li^+] = [Li]_{0.pos} - \frac{Q}{V_{pos} F} \quad (5)$$

$$[Cl^-]_{neg} = [Cl^-]_{0,neg} + \frac{2 * Q}{3 * V_{neg} F} \quad (6)$$

Where $[x]_{0.pos/neg}$ refers to the initial concentration of x on the positive/negative side, Q is the charge passed and $V_{pos/neg}$ are the volumes processed on each side. The acidification at the negative electrode (Eq. 2) shifts the equilibrium between bicarbonate, carbonate, and dissolved CO_2:

$$CO_2(aq) + H_2O \rightleftharpoons HCO_3^- + H^+ \quad (7)$$

$$HCO_3^- \rightleftharpoons CO_3^{2-} + H^+ \quad (8)$$

$$H_2O \rightleftharpoons OH^- + H^+ \quad (9)$$

View Article Online
DOI: 10.1039/D6TA03239G

With corresponding relationships:

$$[CO_2(aq)] = P_{CO2} * C_{Henry} \tag{10}$$

$$[HCO_3^-] = \frac{Ka_1 * P_{CO_2} * C_{Henry} * \gamma_{CO_2}}{\gamma_{HCO_3^-} * \gamma_{H^+}} * \frac{1}{[H^+]} \tag{11}$$

$$[CO_3^{2-}] = \frac{Ka_1 * Ka_2 * P_{CO2} * C_{Henry} * \gamma_{CO2}}{\gamma_{CO_3^{2-}} * \gamma_{H^+}^2} * \frac{1}{[H^+]^2} \tag{12}$$

$$[H^+]\,[OH^-] = K_w \tag{13}$$

where C_{Henry} is Henry's constant, and Ka_1, Ka_2 and K_w are the equilibrium constants for reactions (7) , (8) and (9), respectively. The concentrations re-equilibrate to maintain charge balance in the acidification side:

$$[H^+] + [Na^+] = [Cl^-] + [HCO_3^-] + 2[CO_3^{2-}] + [OH^-] \tag{14}$$

and maintain the total dissolved inorganic carbon (DIC):

$$[DIC] = [CO_2(aq)] + [HCO_3^-] + [CO_3^{2-}] \tag{15}$$

We calculated seawater DIC to be 2.07 mM at pH 8.1 (see SI Section 1.1). Due to seawater's high salinity (S > 0.1), we applied the Dickson and Millero model [23,24] to estimate activity coefficients for the bicarbonate/carbonate system rather than using the Debye-Hückel approach. Additionally, we used the Millero and Schreiber [25] method to estimate activity coefficients for lithium, chloride, and protons based on salinity. The system of equations (5)-(15) is solved for the extraction/acidification step and, similarly, with reversed polarity for the recovery/alkalization step (SI section 1.2 & 1.3).

The speciation of the bicarbonate/carbonate system can be calculated on the bismuth side as a function of charge passed, which results in relatively similar results to a stand-alone Bi/BiOCl carbon capture device [2]. Fig. 2a and Fig. 2b show the speciation of carbonate-containing compounds as a function of charge per volume passed on the bismuth side and the corresponding pH swing, respectively. A pH shift from 8 to 4.5, which requires approximately $Q_{v,neg} = 320\ C/L$, pushes the equilibrium strongly toward $CO_2(aq)$, increasing the partial pressure of CO_2 to 60 mbar and resulting in the extraction of 0.002 mol of CO_2 per liter of processed water, assuming 95% extraction.

Given the desired pH swing target and the fixed charge designed for CO_2 capture, we can calculate how much lithium can be co-extracted, which depends on the initial lithium concentration and the volume processed on the lithium side. Depending on the lithium concentration of the source water, asymmetric residence times between the two sides may therefore be necessary to achieve both the target pH swing and the desired lithium extraction. This asymmetry can be implemented by processing unequal volumes on each side of the cell to meet the different extraction goals. To calculate the required lithium-side volume based on the initial lithium concentration, Eq. (5) can be rewritten as:

$$V_e * [Li]_{0,pos} = \frac{Q_{v,neg}}{SOC * F} \tag{16}$$

View Article Online
DOI: 10.1039/D6TA03239G

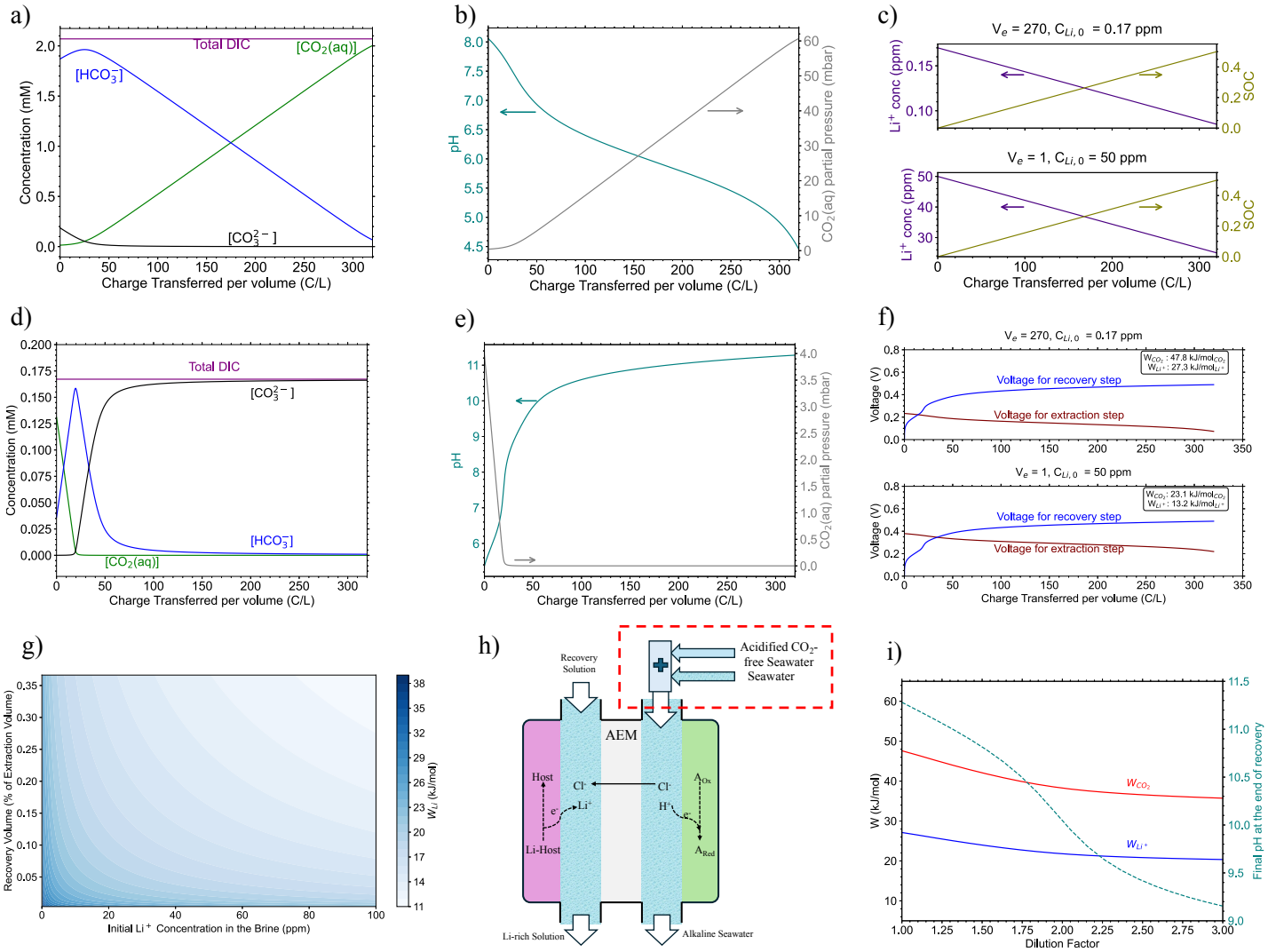

Fig. 2: Thermodynamic and speciation analysis of the dual-function electrochemical system for a dual-function electrochemical cell for simultaneous lithium extraction and carbon capture. ***(a)*** *Speciation of DIC components during the acidification step, showing the shift from bicarbonate and carbonate to aqueous CO_2 as charge is applied.* ***(b)*** *Corresponding pH swing during acidification, and the increase in CO_2 partial pressure.* ***(c)*** *Lithium concentration and state of charge (SOC) on the lithium side during extraction for two representative cases: low-concentration lithium (0.17 ppm, seawater-like, top panel) and high-concentration lithium (50 ppm, brine, bottom panel).* ***(d)*** *Speciation of DIC components during the alkalization (discharge) step.* ***(e)*** *Corresponding pH increase during alkalization, reaching values close to 11 with the same 320 C/L charge input.* ***(f)*** *Voltage profiles for extraction/acidification and recovery/alkalization steps under both lithium concentrations, highlighting the asymmetry in voltage response due to differences in lithium concentration and pH buffering.* ***(g)*** *Contour plot showing the thermodynamic work for lithium recovery as a function of the initial lithium concentration and the lithium-side recovery volume.* ***(h)*** *Schematic of the cell configuration during recovery and alkalization, illustrating how pH on the bismuth side can be controlled by diluting the acidified CO_2-free stream with a fresh seawater stream (i.e. lithium-depleted effluent from the extraction step)* ***(i)*** *Calculated thermodynamic work per mole of CO_2 and Li^+ as a function of the dilution factor on the bismuth side during alkalization, along with the corresponding final pH.*

where V_e is the ratio of the lithium-side processed volume to the bismuth-side volume (V_{pos}/V_{neg}) during extraction and SOC is the desired state of charge on the lithium side (percent depletion of initial lithium). Fig. 2c illustrates the resulting lithium depletion and corresponding V_e values for various initial lithium concentrations. For instance, an initial lithium concentration of 50 ppm (e.g. brine Li concentration) enables 50% SOC with $V_e = 1$, meaning no asymmetry in processed

View Article Online
DOI: 10.1039/D6TA03239G

volumes is needed. In contrast, at 0.17 ppm (representative of seawater Li concentration), a 270× higher volume must be processed on the lithium side to reach the 50% SOC under the same 320 C/L charge input used for the pH swing from 8 to 4.5 on the bismuth side. Importantly, this volume asymmetry does not arise from coupling lithium extraction with carbon capture, but from the inherently dilute concentration of Li^+ in seawater. A stand-alone electrochemical lithium extraction process targeting the same degree of lithium recovery would similarly require processing large volumes of seawater to supply sufficient moles of Li^+. The value of the coupled configuration therefore lies not in requiring equal processing volumes for the two streams, but in enabling lithium extraction and carbon capture to be carried out within a shared electrochemical platform and associated infrastructure. Because the two processes occur in separate streams, their flow rates and processed volumes can be independently selected according to the lithium concentration and the desired DIC conversion.

Assuming 95% of the dissolved CO_2 is extracted during the extraction step, the total DIC drops to approximately 0.167 mM, and the partial pressure of CO_2 falls to 4 mbar. On the lithium side, the electrolyte is replaced with a recovery solution to release the extracted lithium into a smaller volume and generate a concentrated lithium stream. Here, we examine the first fresh recovery stream (i.e., not pre-concentrated). The speciation of the electrolyte during the alkalization step is shown in Fig. 2d, and the resulting pH swing is depicted in Fig. 2e. As can be seen, during alkalization, as the pH shifts to the alkaline region, the equilibrium shifts toward carbonate dominance. Due to the substantial reduction in DIC after extraction, the buffering capacity of the solution decreases, resulting in the same amount of charge (320 C/L) to drive the pH close to 11 during discharge. This asymmetry between the proton and lithium concentrations during extraction/acidification versus recovery/alkalization leads to an observable voltage offset between the two steps, as shown in Fig. 2f for the two lithium concentrations analyzed in Fig. 2c. The corresponding thermodynamic work is calculated using:

$$W_{CO_2} = \frac{\oint V.dQ}{mol_{CO_2}}, W_{Li^+} = \frac{\oint V.dQ}{mol_{Li^+}} \quad (17)$$

This represents the ideal work required for each process, excluding overpotentials and the energetic cost associated with CO_2 stripping. For an initial lithium concentration of 0.17 ppm (seawater-like), the thermodynamic work is 47.8 kJ/mol[1] CO_2, which corresponds to 27.3 kJ/mol Li^+ recovered when the same total work is normalized by the moles of CO_2 captured or Li^+ recovered. In contrast, for a brine with 50 ppm lithium, the work drops to 23.1 kJ/mol CO_2, equivalent to 13.2 kJ/mol Li^+. As expected from the Nernst equation, increasing the initial lithium concentration makes the extraction more favorable, thereby reducing the required work. This trend is shown in Fig. S2, where the energetic cost decreases from 48 to 20 kJ/mol CO_2 (equivalent to 27 to 11 kJ/mol Li^+) as lithium concentration increases from 0.17 to 100 ppm (representing a transition from seawater to brine). Furthermore, during the recovery step, the lithium-side volume is often chosen to be smaller than the extraction-side volume to concentrate on the released lithium. This volume asymmetry affects the Nernst potential during recovery and further increases the energetic cost for highly concentrated streams. As shown in Fig. S3a, reducing the recovery volume from 0.3 to 0.01 times the extraction volume increases the work from 49 to 67 kJ/mol CO_2 (equivalent to 28 to 38 kJ/mol Li^+). Therefore, both the initial lithium concentration and the targeted recovery volume influence the total energy requirement, as summarized in contour plots of Fig. 2g. Additionally, repeated cycling leads to an increase in lithium concentration in the recovery solution, which increases the thermodynamic work required for lithium release as

View Article Online
DOI: 10.1039/D6TA03239G

dictated by the Nernst relation. Figures S3b and S3c quantify the resulting increase in minimum thermodynamic work as the lithium concentration in the recovery stream rises over successive cycles up to 1 M. For an initial brine concentration of 50 ppm Li^+, the required work increases to 53 kJ/mol CO_2 and 30 kJ/mol Li^+, while for seawater (0.17 ppm Li^+) it increases to 77 kJ/mol CO_2 and 44 kJ/mol Li, when the concentration of Li^+ reaches 1 M in the recovery solution.

Another factor affecting energetic cost is the dilution of the bismuth side. During alkalization, the pH can swing to values close to 11 (Fig. 2e). According to the Pourbaix diagram of bismuth [26], this may lead to the formation of Bi_2O_3. To mitigate this, the alkalization step can be adjusted by diluting the bismuth-side solution by mixing with a fresh seawater stream, creating a buffering capacity to control the pH change (Fig. 2h). This stream could be the lithium-depleted effluent from the extraction step. Fig. 2i shows the energetic cost per mole of Li^+ and CO_2 as a function of different dilution factors and the corresponding final pH achieved on the bismuth side.

H-cell Operation

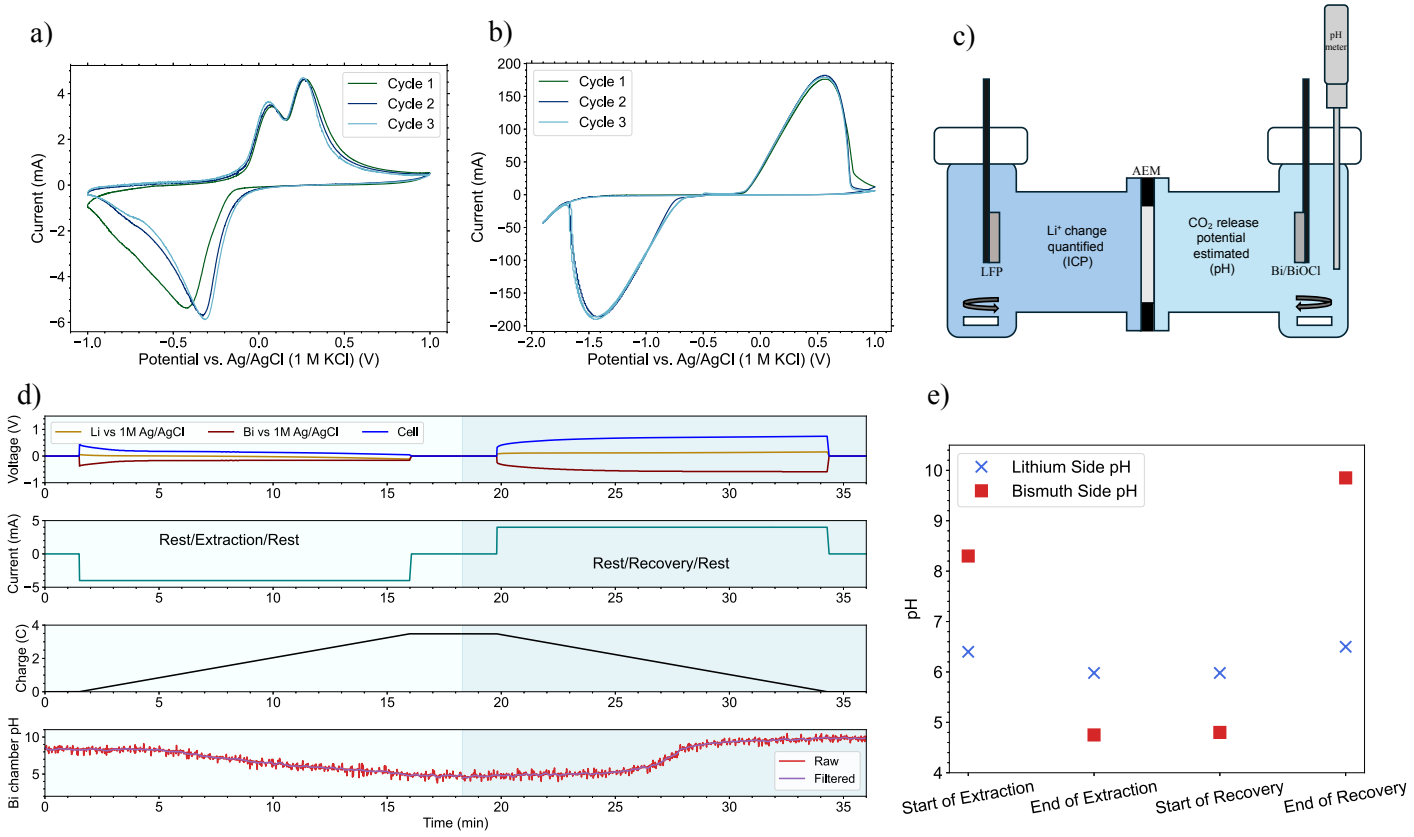

Fig. 3: Half-cell and H-cell studies of the coupled electrochemical CO_2 capture and Li^+ extraction. ***(a)*** *Cyclic voltammograms of the redox-active species on the LFP in 0.5 M NaCl over three cycles at 2 mV/s.* ***(b)*** *Cyclic voltammograms on the bismuth electrode in 0.5 M NaCl over three cycles at 0.2 mV/s.* ***(c)*** *Schematic of the H-cell configuration used for Li^+ extraction and CO_2 capture.* ***(d)*** *Time-resolved electrochemical profiles (overpotential, current, charge) and corresponding pH evolution during the extraction/acidification and recovery/alkalinization sequence. Shaded regions highlight the extraction/acidification and recovery/alkalinization phases.* ***(e)*** *Discrete pH values measured on both sides of the cell at four key stages, illustrating acidification during capture and pH rebound during alkalinization on the bismuth side and minimal pH change on the lithium side.*

View Article Online
DOI: 10.1039/D6TA03239G

Electrochemical characterization of the synthesized LFP and Bi electrodes is performed using cyclic voltammetry (CV). Fig. S4 presents the CV profile of the prepared non-pretreated LFP electrode in 0.5 M LiCl (no Na present), which exhibits distinct lithium deintercalation and intercalation peaks at approximately 0.45 V and −0.08 V vs. Ag/AgCl, respectively. Note that the Li lithiation/lithiation is a one-electron transfer reaction. Fig. 3a presents the CV profiles of a 50% delithiated LFP electrode in the presence of 0.5 M NaCl, which demonstrates additional redox features, indicating concurrent sodium intercalation/deintercalation. Upon reduction, a new prominent peak appears at −0.44 V vs. Ag/AgCl, attributed to sodium intercalation alongside the lithium reduction peak at −0.05 V vs. Ag/AgCl. During oxidation, prominent peaks at 0.03 V and 0.28 V vs. Ag/AgCl are observed, corresponding to lithium and sodium deintercalation. Additional overlaid CV profiles for 350 ppm lithium in the presence and absence of 0.5 M NaCl further demonstrate the concurrent Na and Li reactions (Fig. S5). Such competing intercalation behavior under mixed-ion conditions has been reported in the literature [27,28]. For the Bi electrode (Fig. 3b), the CV profiles remain stable over the cycles. Note that Bi/BiOCl is a three-electron transfer reaction. Characteristic peaks at 0.55 V and −1.44 V vs. Ag/AgCl are associated with the reversible Bi/BiOCl conversion.

To assess the feasibility of coupling lithium extraction and CO_2 capture, an H-cell configuration was employed (Fig. 3c and Fig. S6), with compartments separated by an anion exchange membrane (Selemion DSVN). Due to the limited electrolyte volume in the H-cell, a solution containing 0.25 mM DIC was used on the bismuth side, and 350 ppm lithium on the lithium side, both in 0.5 M NaCl. Higher DIC concentrations and lower lithium concentrations will be tested in a flow-cell design where volume control is more flexible. The cell was operated at a constant current density of 1.0 mA/cm^2. On the bismuth side, the pH decreased from 8.3 to 4.7 during acidification, rose slightly to 4.8 after resting, and increased to 9.8 following alkalization. This behavior is consistent with CO_2 capture during acidification and the reduced buffering capacity at low DIC concentrations during alkalization, as predicted by the thermodynamic analysis. In DIC-free controls, the pH on the bismuth side fully returned to baseline after cycling, with no observable change on the lithium side (Fig. S7). Additionally, the lithium side also showed no significant pH shift, with measurements before and after extraction and recovery remaining between 6.0 and 6.4 (Fig. 3e). Inductively coupled plasma (ICP) analysis confirmed the extraction of 25.3 μmol of lithium, corresponding to a lithium capacity utilization of 70%, where capacity utilization is defined as the fraction of the total charge passed that is attributed to Li^+ transport. Assuming the remaining charge is carried by Na^+, as supported by the cyclic voltammetry profiles, this corresponds to an effective Li/(Na+Li) charge selectivity of 70%. This preliminary H-cell experiment validates the fundamental compatibility of the two half-reactions and provides the basis for subsequent integration in a flow cell architecture.

Flow Cell Operation

An electrochemical flow cell (Fig. 4a) was assembled with an LFP electrode paired with a bismuth electrode to demonstrate coupled CO_2 capture and Li^+ extraction, beginning with brine-relevant lithium concentrations (See SI Section 4.1). The lithium side contained 25 mL of 50 ppm Li^+ in 0.5 M NaCl, while the bismuth side contained 25 mL of 1.91 mM $NaHCO_3$ + 0.19 mM Na_2CO_3 (total DIC: 2.1 mM; seawater DIC as described in SI Section 1) in 0.5 M NaCl. Given the initial lithium concentration of 50 ppm in this test, no asymmetry in processed volumes is required (Eq. 16). The compartments were separated by an anion exchange membrane with continuous N_2 flow in the bismuth reservoir for CO_2 purging. A constant current density of 1 mA/cm^2 was applied.

View Article Online
DOI: 10.1039/D6TA03239G

Both the total cell voltage (LFP–Bi) and LFP potential vs Ag/AgCl were monitored. The bismuth electrode potential was obtained by subtraction and is therefore approximate due to uncompensated internal resistance.

The extraction/acidification step concluded when the bismuth-side pH decreased from 8.0 to 4.5-4.8, triggering CO_2 desorption. The cell was then held at open-circuit potential to allow the CO_2 sensor to register and stabilize. After rinsing the lithium side with distilled water, a recovery solution is recirculated containing 20 mL of 0.05 M KCl + 0.14 ppm Li^+, which was reused across cycles to progressively concentrate the lithium stream. On the bismuth side, the CO_2-degassed electrolyte was mixed with 100 mL of pristine solution to increase buffering capacity and avoid exceeding pH 10 during recovery (see discussion in Fig. 2h). In practice, this pristine solution can be the lithium-deficient seawater electrolyte previously used on the lithium side (Fig. S11).

View Article Online
DOI: 10.1039/D6TA03239G

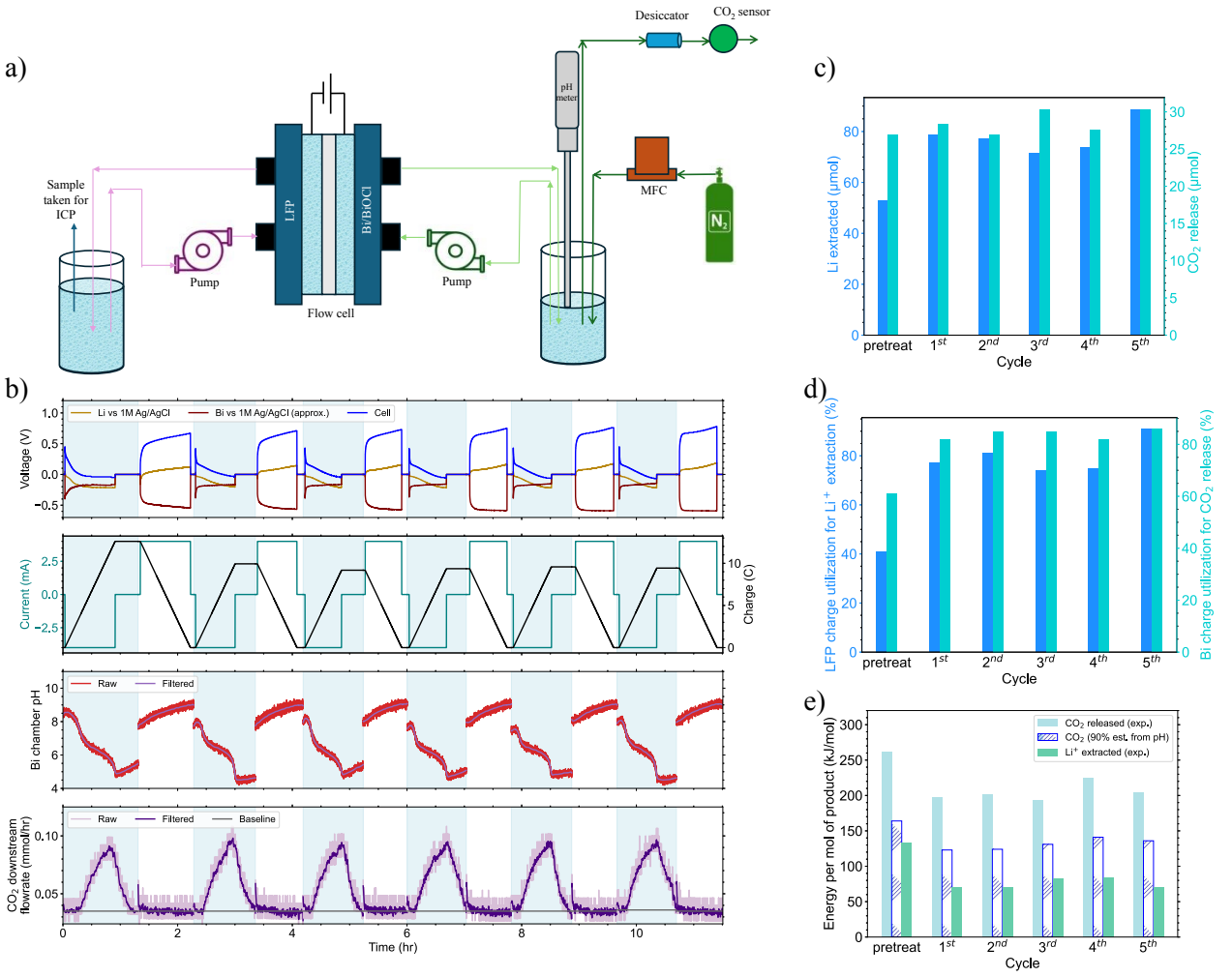

Fig. 4: Full-cell performance of the coupled electrochemical CO_2 capture and Li^+ extraction flow system at 50 ppm Li^+ and 2.1 mM DIC (no impurities). *During extraction/acidification, the lithium side contained 25 mL of 50 ppm Li^+ in 0.5 M NaCl, and the bismuth side contained 25 mL of 1.91 mM $NaHCO_3$ + 0.19 mM Na_2CO_3 in 0.5 M NaCl. During recovery/alkalization, the lithium side was supplied with 20 mL of 0.05 M KCl + 0.14 ppm Li^+, which was reused across cycles to concentrate the lithium stream. On the bismuth side, the CO_2-degassed electrolyte from acidification was mixed with 100 mL of pristine solution to increase buffering capacity.* ***(a)*** *Schematic of the electrochemical flow setup.* ***(b)*** *Voltage, current density, pH (measured on the bismuth side), and CO_2 downstream flow rate on the bismuth side over five operation cycles.* ***(c)*** *Amount of Li extracted (from ICP measurements, converted to µmol) and CO_2 detected (from CO_2 sensor measurements, converted to µmol) for each cycle.* ***(d)*** *Charge utilization at the lithium and bismuth electrodes.* ***(e)*** *Energy per mole of product, calculated by dividing the total energy consumed by the moles of CO_2 captured (from sensor data), the moles of CO_2 estimated from 90% achievable pH swing, and the moles of Li extracted (from ICP measurements) for each cycle.*

The first cycle served as a pretreatment step for further electrode activation, resulting in lower utilization of both electrodes (Bi utilization: 60%, Li utilization: 44%) and requiring 20% more charge to reach the same pH endpoint. Subsequent cycles showed higher and stable utilization (Bi: 84%, Li: 78% on average). This five-cycle protocol produced the voltage, current, bismuth-side pH, and CO_2 data shown in Fig. 4b, with lithium-side pH values before and after each cycle provided in Fig. S11 and S12. ICP analysis confirmed an average lithium extraction of 78 µmol per cycle, corresponding to an average of 78% charge utilization on the lithium side toward lithium extraction (Figs. 4a and 4b). Simultaneously, CO_2 sensor data indicated an average CO_2 release of

View Article Online
DOI: 10.1039/D6TA03239G

29 μmol per cycle. The bismuth-side pH during acidification decreased from 8.5 to 4.5-4.8, corresponding to 84% charge utilization toward pH change (Figs. 4a, 4b). The lithium-side pH increased slightly from 6.5 to 7.7 before and after extraction.

During alkalization, the bismuth-side pH (after mixing with pristine solution) increased to 8.5 and only reached 9.0 at the end of the step, successfully avoiding pH > 10, which could lead to the formation of Bi_2O_3 [26]. The lithium-side pH remained negligible between 7.1 and 7.7 during recovery. The average energetic cost across cycles was 204 kJ/mol CO_2, equivalent to 75 kJ/mol Li. In addition to these values, we report an estimate based on 90% of the CO_2 capture predicted from the pH swing achieved in the experiments (from 8.5 to 4.5-4.8). The CO_2 detected by the sensor under N_2 degassing was lower than the amount predicted from the pH swing. In a practical configuration integrating a membrane contactor, which is a more efficient CO_2 degassing method, and a higher-sensitivity CO_2 analyzer, 90% of the predicted CO_2 captured should be recoverable. Using this achievable degassing efficiency, the electrochemical energetic cost is estimated at 131 kJ/mol CO_2.

Next, major ionic impurities commonly present in seawater (Mg^{2+}, Ca^{2+}, and K^+) were introduced at typical seawater concentrations (Table S2). Our preliminary tests indicated that, after the first cycle, the pH drop on the bismuth side was delayed in the presence of these impurities, with an initial increase in the pH before the expected decrease (Fig S13), which was more significant than the case without impurities. This behavior suggests that a fraction of the acid generated during acidification was consumed prior to bulk acidification. Given that the bulk solution pH was maintained below 10, under which conditions $Mg(OH)_2$ and $Ca(OH)_2$ precipitation should be thermodynamically unfavorable, we propose two possible explanations for this behavior. First, local pH spikes at the electrode surface may transiently exceed the solubility thresholds, forming $Mg(OH)_2$ or $Ca(OH)_2$ that subsequently dissolve during the acidification step, consuming protons and delaying the pH swing. Second, based on the Ksp data (See SI Section 4.3 and Table S4) and the seawater composition (Table S2), the ionic products of $MgCO_3$ and $CaCO_3$ exceed their Ksp values, indicating that their precipitation is thermodynamically favored. Re-dissolution of these transient carbonate phases during acidification would consume protons and increase the charge required for an equivalent pH swing. To mitigate these impurity-driven effects, we implemented a modified operating strategy in which the acidified electrolyte from CO_2 degassing was collected and used to wash the cell prior to each acidification step. Alkalization was then carried out using only pristine seawater, rather than the previous approach of mixing acidified and pristine solutions (See Fig. S14). This acid-washing approach reduced the delay in the pH drop and the associated proton consumption, although both remained moderately higher than in the impurity-free condition (See Fig. S15). The bismuth-side flow rate was also increased from 35 to 60 ml/min to facilitate the removal of transient precipitates and reduce local pH excursions (see Table S3).

Fig. 5 summarizes system performance at 50 ppm Li^+ in the presence of impurities, with acid washing (retained from the acidified solution during acidification) implemented between cycles. As anticipated from the preliminary tests, the first cycle exhibited a pH swing similar to impurity-free conditions. In subsequent cycles, however, the pH drop on the bismuth side was delayed, showing an initial increase before decreasing (see inset in Fig. 5c). This delay resulted in a higher charge requirement to achieve a comparable pH swing, for example, 9 C was required to lower the pH from 7.9 to 4.5 under impurity-free conditions, whereas 12.4 C was required under impurity-containing conditions for a similar pH change. In the presence of impurities, bismuth-side charge utilization for the pH swing stabilized at 60% (Fig. 5b). Although this value is lower than the 84%

View Article Online
DOI: 10.1039/D6TA03239G

utilization observed without impurities (Fig. 4), it is substantially higher than previously reported values for bismuth electrodes operated with similar impurities at 1 mA/cm^2, where utilization declined to 20% by the second cycle and 10% by the fourth cycle [2]. These results indicate that acid washing effectively preserves reasonable utilization under impurity-containing seawater conditions.

Throughout cycling, the pH evolution on both the bismuth and lithium sides followed the expected trends, with the bismuth-side pH decreasing from 8.1 to 4.5 during acidification, while the lithium-side pH exhibited negligible change (Fig. S16). During recovery, a slightly alkaline pH was observed on the lithium side (8.6 compared to 7.8 in the absence of impurities (Fig. S19)), which

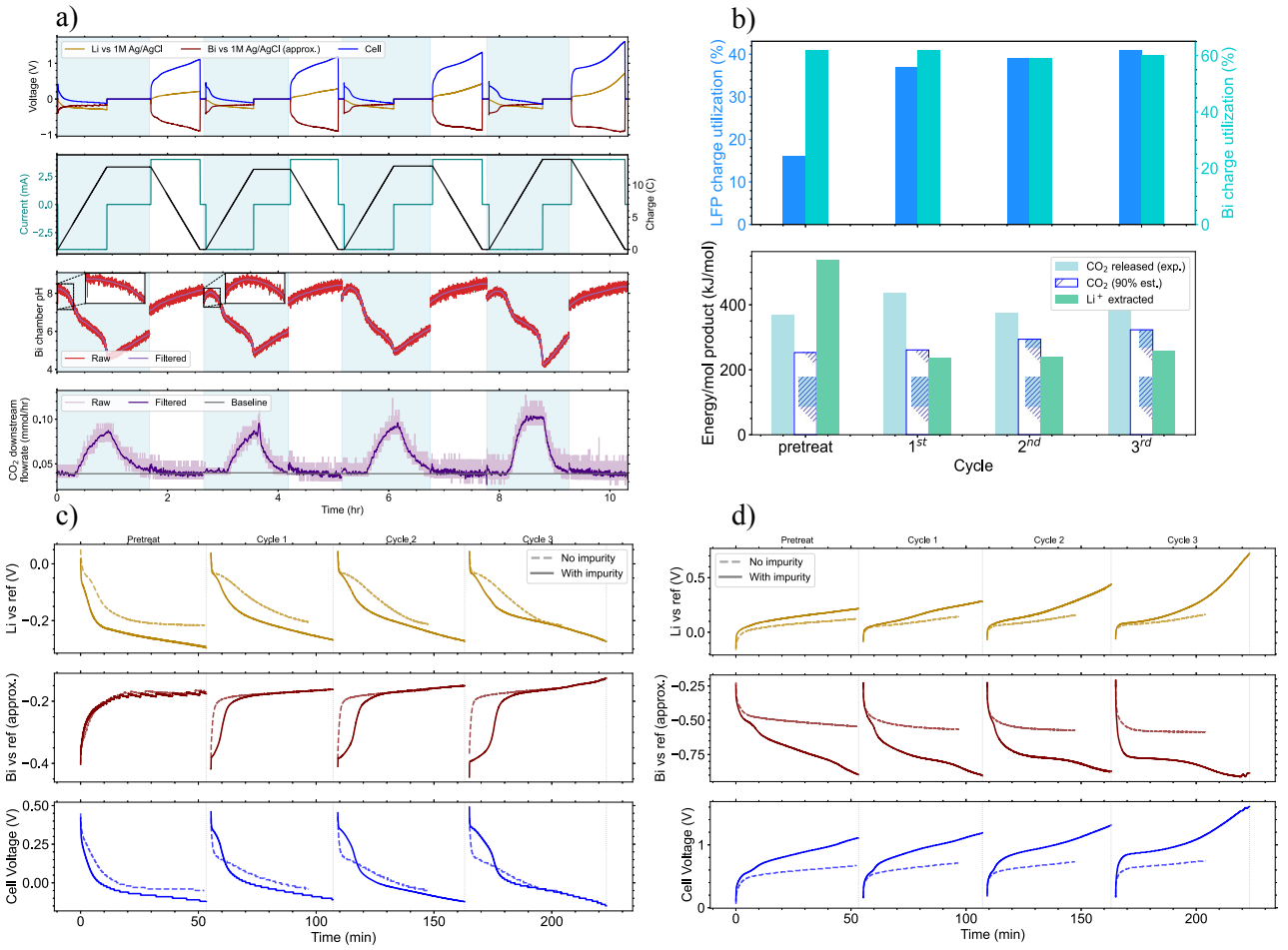

Fig. 5: Electrochemical CO_2 capture–Li^+ extraction cycling performance at 50 ppm Li^+ and 2.1 mM DIC (with impurities). *The cell configuration was identical to Fig. 4, with impurities added as listed in Table S1. During recovery, 20 mL of 0.05 M KCl with 0.17 ppm Li^+ was reused to progressively concentrate lithium, while 100 mL of pristine seawater with impurities restored buffering on the bismuth side for alkalization. Between cycles, the system was rinsed with DI water, and the acidified spent electrolyte was used for washing the bismuth side.* ***(a)*** *Full-cell cycling behavior during cycling, showing electrode potentials vs Ag/AgCl, applied current and charge, and CO_2 concentration at the bismuth reservoir gas outlet.* ***(b)*** *Li^+ and Bi utilization per cycle (top) and energy consumption per mole of product (bottom).* ***(c)*** *Electrode potential responses during extraction/acidification cycles with and without seawater-derived impurities.* ***(d)*** *Electrode potential responses during recovery/alkalinization cycles with and without seawater-derived impurities.*

is attributed to the presence of co-intercalated seawater cations that undergo partial de-intercalation

View Article Online
DOI: 10.1039/D6TA03239G

during the recovery step. ICP confirmed simultaneous lithium extraction that increased over cycles, yielding an average lithium-side charge utilization of 40%, markedly lower than the 78% obtained in the absence of impurities. The energetic cost calculated for each cycle is shown in Fig. 5b, with averages of 245 kJ/mol Li, 399 kJ/mol CO_2, and 292 kJ/mol CO_2 when normalized to 90% of the thermodynamically predicted CO_2 capture. The increase in energetic cost in the presence of impurities can be understood by analyzing the electrode potential and cell voltages in Fig. 5c and d.

As shown in Fig. 5c, during extraction the lithium intercalation potential shifts to more negative values in the presence of impurities, while the bismuth potential remains largely unchanged. Driving the lithium electrode to these more negative potentials enables Na^+ and other cations co-intercalation in addition to Li^+, which explains the reduced lithium utilization observed in Fig. 5b (consistent with Na^+ insertion becoming accessible at more negative potentials, Fig. S5). Meanwhile, the acidic environment on the bismuth side during acidification suppresses local hydroxide or carbonate precipitation, allowing a similar extraction potential on the bismuth side to the impurity-free case. During recovery/alkalinization (Fig. 5d), the presence of impurities affects both electrodes. Because less Li^+ was intercalated during extraction, while other cations were intercalated, de-intercalation becomes more difficult, leading to a shift to a more positive potential. Simultaneously, the higher pH on the bismuth side during alkalinization increases the likelihood of transient hydroxide/carbonate formation, which perturbs the bismuth potential and increases overpotential. Together, these shifts lead to higher cell voltages and, consequently, increased energetic cost under impurity-containing conditions.

At lower lithium concentrations, the performance trends observed at 50 ppm in the presence of impurities are expected to become even more pronounced (See Fig. S17). To address these challenges, additional modifications were implemented before operating the cell at lower lithium concentrations close to seawater. A voltage-pulsed extraction protocol was introduced to enhance diffusion of reactants to the electrode surface and to remove accumulated reaction products. Prior studies have shown that pulsed operation can improve the selective electrochemical extraction of uranium [29] and lithium [12]. In the present system, it may also facilitate bismuth oxidation to BiOCl by reducing the diffusion layer thickness for chloride transport to active sites. The applied sequence of pulsed–reverse-pulse protocol (P-RP) consisted of 10 s of constant current, followed by 10 s at open circuit, then 2 s of reverse pulse, and 2 s at open circuit and only applied to the extraction/acidification step. The recovery/alkalinization step, which is non-spontaneous and energy-requiring, was performed under standard constant-current operation. In addition, based on previous reports demonstrating improved Li^+ selectivity with TiO_2 modification [12], the lithium electrode was coated with a ≈3 nm TiO_2 layer to further suppress other cations co-intercalation (details in SI Section 4.4).

Fig. 6a shows the system performance at 5 ppm Li^+ with 2.1 mM DIC, 0.17 ppm Li^+ with 2.1 mM DIC, and 0.17 ppm Li^+ with 2.1 mM DIC and added seawater impurities, progressively demonstrating performance as the operating conditions approach those of real seawater. To enable lithium extraction while still achieving the required pH swing at these lower lithium concentrations, we implemented an asymmetric flow operation strategy (Eq. 16, Fig. S18). During extraction/acidification, 250 mL and 7.5 L were processed on the lithium side for the 5 ppm and 0.17 ppm Li^+ conditions, respectively, paired with 25 mL on the bismuth side. During recovery and alkalinization, as before, asymmetric volumes (20 mL lithium side, 125 or 100 mL bismuth

View Article Online
DOI: 10.1039/D6TA03239G

side based on impurity presence) were used to concentrate lithium and maintain buffering capacity on the bismuth side.

Across all runs in Fig. 6a, pH-swing was successfully coupled with lithium extraction. The bismuth side consistently achieved a pH swing from 8.2 to 4.7 during acidification, while the recovery pH remained below 10 (typically ≈9). The lithium-side pH remained relatively unchanged between 6-7.5 throughout all cycles in absence of impurities and remained at around 9.5 when the impurities are included, since the intercalated impurities are released into the recovery, increasing the recovery solution pH (Fig. S19). ICP analysis showed average lithium utilization of 66%, 54%, and 29% for the 5 ppm Li^+, 0.17 ppm Li^+, and 0.17 ppm Li^+ with impurities cases, respectively. Corresponding bismuth utilization based on the pH swing was 77%, 85%, and 60%, respectively.

Energy-Dispersive X-ray Spectroscopy (EDX) area quantitative analysis (carbon excluded) of the bismuth electrodes before and after operation under seawater-relevant conditions (0.17 ppm Li^+, 2.1 mM DIC with impurities) shows pronounced impurity accumulation on the cycled electrode, including 6.0 ± 0.3 at% Mg and 0.7 ± 0.3 at% Ca, which were undetectable in the pristine sample, accompanied with the increase in oxygen atomic percentage by 12.6 ± 1.1 at%. This is consistent with the formation of Mg or Ca precipitates as hydroxide or carbonate during the alkalization step, leading to surface deposition on the Bi electrode. On the lithium electrode, Na (1.7 at%), Mg (1.2 ± 0.1 at%), Ca (1.6 at%), and Cl (0.6 at%) were present only after cycling. Given the intercalation-based operation of this electrode, these species are attributed to a combination of co-intercalation and surface accumulation, rather than pH-driven precipitation. These results indicate that seawater-derived divalent cations, particularly Mg^{2+}, form surface deposits (bismuth side) or intercalate (lithium side) during operation and thereby reducing utilization on both sides of the cell. The acid washing and pulsated operation partially restored performance; however, further improvements, such as pretreatment steps to temporarily bind or remove Mg^{2+} or Ca^{2+}, may be required for fully integrated seawater operation. To isolate the lithium-extraction performance from impurity impacts, we next operated the system at seawater-level lithium (0.17 ppm Li^+) with identical DIC (2.1 mM) but without seawater impurities, and extended cycling to five extraction–recovery cycles. Stable utilization values of 85% on the bismuth side and 54% on the lithium side were achieved (Fig. 6d). Consistent pH swings were maintained between 8.1-8.5 to 4.7-5.0 during extraction, with negligible pH change on the lithium side (See SI Section 4.5). The average energetic cost was 121 kJ/mol Li, 172 kJ/mol CO_2, and 128 kJ/mol CO_2 when normalized to 90% of the thermodynamically predicted CO_2 capture (Fig. 6e). To enable direct comparison across all tested conditions, capacity utilization and energetic costs are summarized in Fig. 6d and 6e, respectively, and the corresponding voltage profiles are overlaid in SI Section 4.6.

As seen in Fig. 6d, across all lithium concentrations, bismuth utilization remains high at 80% when impurities are absent, consistent with the expectation that lithium concentration on the LFP side should not influence the bismuth-side utilization. However, when seawater impurities are introduced, bismuth utilization decreases to 60%, which is still higher than previously reported stand-alone system with bismuth electrode in the presence of impurities [2]. In contrast, lithium utilization decreases from 80% at 50 ppm to 50% at 0.17 ppm and further dropping to 30% when impurities are present. The major performance penalty appears only when impurities are present.

View Article Online
DOI: 10.1039/D6TA03239G

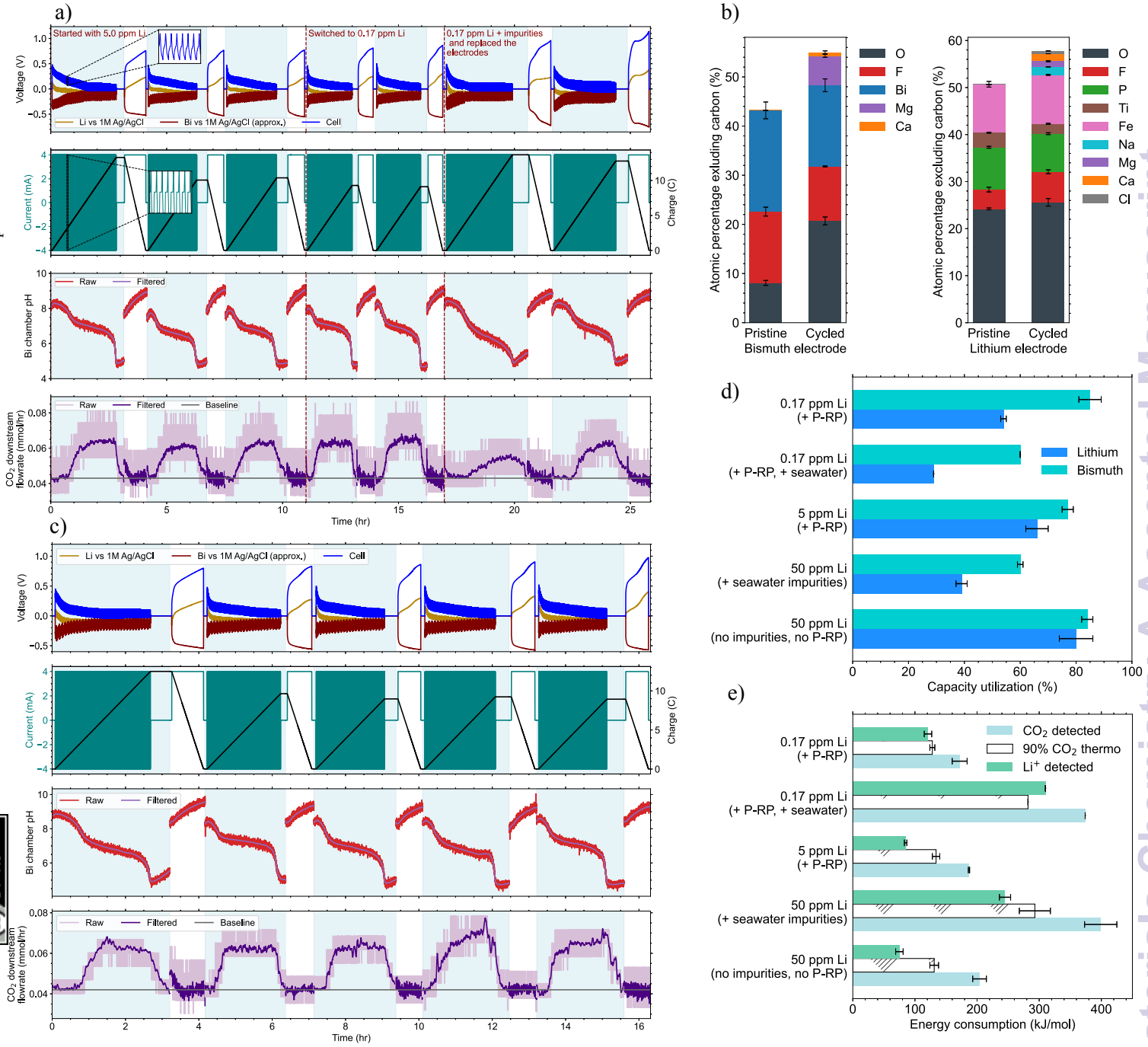

Fig. 6: Electrochemical CO_2 capture–Li^+ extraction cycling performance under seawater-relevant conditions with and without impurities. ***(a)*** *Full-cell cycling behavior under three scenarios: (i) 5 ppm Li^+, (ii) 0.17 ppm Li^+, and (iii) 0.17 ppm Li^+ with seawater-derived impurities. Extraction and acidification step was operated using 10 s forward pulse + rest and 2 s reverse pulse + rest at 1 mA/cm² , using 250 mL of 5 ppm Li^+ or 7.5 L of 0.17 ppm Li^+ extraction solution. Recovery and alkalization step was performed at 1 mA/cm² using 20 mL of 0.05 M KCl containing 0.17 ppm Li^+, reused across cycles to progressively concentrate lithium. The bismuth side used 25 mL simulated seawater during extraction, with 100 mL pristine solution added during recovery to restore buffering capacity. Shown are voltage vs Ag/AgCl, applied current/charge, bismuth potential, and CO_2 outlet concentration.* ***(b)*** *EDX area analysis of bismuth and lithium electrodes before and after cycling for the 0.17 ppm Li^+ (7.5 L) condition with seawater impurities.* ***(c)*** *Cycling performance with 0.17 ppm Li^+ in the absence of seawater-derived impurities for comparison.* ***(d)*** *Capacity utilization of Li^+ and Bi across all electrolyte conditions.* ***(e)*** *Energy consumption per mole of product for each condition (Li^+ detected, and CO_2 detected vs thermodynamic).Common to labels in d–e: Li electrolyte = 0.5 M NaCl; Bi electrolyte = 2.1 mM DIC; P-RP = pulsed–reverse-pulse protocol.*

The voltage profiles (Fig. S23-S26) corroborate this, showing that voltage losses correlate directly

View Article Online
DOI: 10.1039/D6TA03239G

with Mg or Ca-rich conditions rather than low lithium concentration.

Energetically (Fig. 6e), attractive energy costs are obtained for both CO_2 release and Li^+ extraction, where the dual-function system performs similarly to or better than previously reported stand-alone systems. To contextualize these results, Table 1 compares the energetic performance of this dual-function platform with stand-alone electrochemical carbon capture systems, where protons are generated via water splitting or redox-active species, and lithium extraction systems based on electrochemical intercalation or membrane technologies from saline waters. For fair comparison, differences in current density, lithium concentration, DIC concentration, and the presence or absence of impurities must be considered. In carbon-capture mode, the most relevant benchmark (excluding architectures requiring precious metal catalysts such as Pt or Ru) is a Bi paired with Ag/AgCl pH-swing system operated at similar DIC and current density [2], where the reported energy cost of 122 kJ/mol CO_2 closely matches our 128 kJ/mol CO_2 under the same impurity-free operation. This confirms that adding lithium-extraction functionality does not compromise carbon-capture performance.

For lithium extraction, the closest prior report achieves energetic costs of 653 [30] and 438 kJ/mol Li [31] at current densities that are 33-fold and 5-fold lower than those used here, respectively. Under our operating current density of 1 mA/cm^2 , we obtain 121 and 310 kJ/mol Li in impurity-free and simulated-seawater conditions, respectively, demonstrating substantially lower energetic costs despite the higher operating current density. Although a minimum value of 63 kJ/mol Li is cited in the table [32], this was achieved at lithium concentrations approximately three times higher and at nearly 100-fold lower current density, highlighting that our energetic performance remains highly competitive. Collectively, these comparisons show that simultaneous CO_2 capture and lithium extraction can be achieved within a single saline-water electrochemical system while maintaining energetic efficiencies that meet or exceed those of stand-alone technologies.

Note that $LiFePO_4$ paired with a Bi/BiOCl electrode is used here as a representative material system; however, as lithium-selective host materials and PCET electrodes continue to emerge, they can be readily integrated within this framework. From a deployment perspective, a near-term implementation is expected to employ brine on the lithium side paired with seawater on the carbon capture side, while lithium extraction from dilute sources such as seawater is anticipated to become feasible as more selective materials are developed [12]. For any materials selected within this concept, long-term stability remains an important consideration for practical deployment; however, meaningful extended cycling studies require automated laboratory setup. The automation system must coordinate the operation of the potentiostat, pumps, valves, and sensors to control current application based on pH and CO_2 sensor feedback while managing electrolyte exchange between brine and recovery solutions on the lithium side, and between acidification and alkalization solutions on the carbon capture side. In addition, automated mixing and acid-washing protocols will be required to mitigate precipitate accumulation and maintain stable long-term continuous cycling. This enables systematic pre- and post-characterization of the electrodes under relevant operating conditions. Finally, the influence of impurities inherent to seawater and brines may be mitigated through impurity-tolerant electrode designs, improved flow-field architectures

View Article Online
DOI: 10.1039/D6TA03239G

to suppress local pH spikes, or targeted pretreatment of the source water prior to the electrochemical operation.

Conclusions

In this work, we demonstrate a proof-of-concept dual-function electrochemical system capable of coupling CO_2 capture and Li^+ extraction from saline waters within a single device. Using a pH-swing architecture with bismuth and $LiFePO_4$ electrodes, the system achieves stable pH cycling between 8.1 and 4.7 at 2.1 mM dissolved inorganic carbon, while enabling lithium extraction across a wide concentration range spanning brine-relevant levels (50 ppm Li^+) down to seawater-relevant concentrations (0.17 ppm Li^+). We demonstrated that employing asymmetric flow operation with mismatched electrolyte volumes enables independent pH control on the bismuth side through controlled mixing of acidified and pristine seawater, while allowing lithium to be concentrated on the lithium-intercalation side by using a lower-volume recovery stream. In addition, operational strategies such as pulsed–reverse-pulse operation during extraction and periodic acid washing further improved system performance.

Under impurity-free conditions, the system maintains 80% bismuth utilization and 50% lithium utilization, with energetic costs of 128 kJ/mol CO_2 and 121 kJ/mol Li, respectively, comparable to or exceeding the performance of previously reported stand-alone systems without reliance on precious-metal catalysts. When benchmarked under more challenging impurity-containing conditions, the system remains highly competitive, achieving 282 kJ/mol CO_2 and 310 kJ/mol Li at an operating current density of 1 mA/cm^2, compared to prior reports that require substantially lower current densities to reach similar performance.

Future work should focus on improving the selectivity of lithium host electrodes toward Li^+, particularly for dilute sources such as seawater, and on developing fully automated laboratory setups to enable long-term operation of selected material systems. Tolerance to impurities present in brines and seawater will also be critical and may be addressed through the design of impurity-tolerant electrodes or through targeted pretreatment of saline feedwaters prior to electrochemical operation. Beyond the specific material system examined here, this work introduces a broader way of thinking about electrochemical carbon capture systems. From the perspective of carbon capture technologies, coupling CO_2 capture with lithium extraction introduces an additional co-value stream and an opportunity to generate revenue directly at the capture stage. From the perspective of lithium recovery, integration with a comparatively more mature carbon capture framework broadens potential deployment pathways by increasing the overall incentive to pursue lithium extraction technologies.

Table 1: Comparison of electrochemical systems used for carbon dioxide or lithium extraction

Configuration	Electrode used	Cell voltage E^0 (V)	Current density (mA/cm^2)	Electrolyte composition (mM)									Net Energetic Cost, Cell, (kJ/mol)[a]
				Na^+	Mg^{2+}	Ca^{2+}	K^+	Li^+	DIC	Cl^-	SO_4^{2-}	Br^-	
Carbon dioxide Extraction													
Bipolar membrane Electrodialysis [3]	Ti with IrO_2-RuO_2 coating	1.64	1.24	417	56.7	11.8	9.10	0.09	3.11	505	14.8	1.19	242

View Article Online
DOI: 10.1039/D6TA03239G

Bipolar membrane Electrodialysis [5]	Ti plates with Pt coating	0.83	3.30	417	56.7	11.8	9.10	0.09	3.11	505	14.8	1.19	155
Electrochemical Hydrogen Looping [4]	Carbon paper with Pt coating	0.83	8.00	502.5	-	-	-	-	2.50	500	-	-	104
Electrochemical asymmetric chloride-mediated [2]	Graphite sheet with Bi and Ag coating	0.07	1.00	502.5	-	-	-	-	2.50	500	-	-	122
Dual-function electrochemical cell *(This work)*	Graphite sheet with Bi and LFP coating	0.20	1.00 [f]	502	-	-	-	-	2.10	500	-	-	128
				502	54.0	10.0	10.0	0.02	2.10	638	-	-	282
Lithium Extraction													
Intercalation deionization cell [33]	Carbon cloth with & without LFP coating	0.36	0.099	3,100	-	1,070	540	42.0	-	5,822[b]	-	-	101
Decoupled & membrane-free [34]	Ti mesh with $LiFePO_4$ and Ag coating	0.00	2.50	73.8	2,682	614	34.7	6.7	-	6,599	-	108	75.8
Fluidic electrochemical extraction [35]	MnO_2 coated on a graphite plate, and carbon felt	0.10	0.125	472	54.3	9.98	8.95	1.0	2.83	550	27.7	27.7	181
Membrane-free extraction from desalination brine [32]	Graphite sheet λ-MnO_2 and Ag coating	0.91	0.01[c]	1,146	133	25.7	25.5	0.063	-	1,488	-	-	62.5
Three-chamber cell with glass-type membrane[d] [30]	Pt-Ru and hollow fibre Cu	1.76	0.03	537	64.4	12.1	19.1	0.030					653
Aqueous-Organic cell with lithium-ion exclusive channels [31]	NiO coated on carbon cloth and Cu	1.68	0.2	409	49.8	N/A[e]	8.52	0.028		N/A [e]			438
Dual-function electrochemical cell *(This work)*	Graphite sheet with Bi and LFP coating	0.20	1.00 [f]	500	-	-	-	0.024	-	500	-	-	121
				502	54.0	10.0	10.0	0.024	2.10	638	-	-	310

[a] Net energy of the electrochemical system excluding pumps and other electrical equipment
[b] Not specified in the paper explicitly
[c] Reported current density is during extraction. The release was done at 0.2 mA/cm^2
[d] Reported the first extraction step where seawater is used as a feed. The following cycles used the concentrated lithium solution for further refinement
[e] Seawater was used, but the anions concentrations were not available
[f] A constant current of 1.00 mA/cm^2 was applied during the recovery/alkalinization step, which is the energy-requiring process. The extraction/acidification step was conducted under pulsed operation

Methods

Chemicals. All chemicals were used as received. Lithium iron phosphate (LFP, MTI Corp), bismuth (Bi 99.9%, 100m, SkySpring Nanomaterials Inc), super P conductive carbon black (C, MTI Corp), polyvinylidene fluoride (PVDF, Sigma-Aldrich), N-Methylpyrrolidone (NMP, > 99.0%, Sigma-Aldrich), lithium chloride (LiCl, > 99%, Thermo Scientific), sodium chloride (NaCl, >99%, Fisher Chemical), potassium chloride (KCl, > 99%, Fisher Chemical), magnesium chloride hexahydrate ($MgCl_2.6H_2O$, >99%, Sigma-Aldrich), calcium chloride dihydrate ($CaCl_2.2H_2O$, VWR), sodium bicarbonate ($NaHCO_3$, >99.7%, Sigma-Aldrich), sodium carbonate (Na_2CO_3, Sigma-Aldrich), and nitric acid (HNO_3, >99.999%, Sigma-Aldrich)

Electrodes preparation. A slurry mixture of active material (LFP or Bi), conductive material (carbon black) and binder (PVDF) is mixed with the solvent, NMP. The mixture is cast on a Sigracet 28AA carbon paper (Fuel Cell Store), and placed in a vacuum oven (Across International) for drying. Slurry composition, material loading and other additional information are available in supplementary information (See Supplementary Section 2.1).

Pretreatment & Cyclic Voltammograms. A 100 ml H-cell is used with a 1M Ag/AgCl reference electrode, graphite rod counter electrode (6.35 mm, Electron Microscopy Sciences) and an anion exchange membrane (AEM, Selemion

View Article Online
DOI: 10.1039/D6TA03239G

DSVN). All experiments were run using the 2 channel Biologic SP-300 potentiostat in floating mode. The pretreatment and cyclic voltammogram for LFP and Bi electrodes are different and are available in supplementary information (See Supplementary Section 2.2).

H-cell experiment. Similar setup is used when pairing LFP and Bi electrodes in the H-cell. A multi-position and hot plate at 700 rpm (BT Lab Systems) is used for homogenous mixing, while pH measurements are taken using a pH probe (Mettler Toledo LE422). To purge out aqueous CO_2 formed during extraction, 30 sccm N_2 is bubbled into the bismuth solution using a mass flow controller (Sierra). To control electrical components and record readings, an Arduino board with a data logger software (CoolTerm) is used. Image of the setup, experimental procedure and additional information is available in the supplementary information (See Supplementary Section 3)

Flow-cell experiment. A 5cm^2 flow cell hardware (Fuel Cell Technologies) is used for the zero gap flow cell experiments, with the Viton gaskets (McMaster) cut to match the cell window. Diaphragm pumps (FF 12 DCB-4', KNF) are used to circulate the electrolyte, flow sensor (FS4001,Siargo Ltd) is used to ensure gas flow in the bismuth reservoir outlet gas line and CO_2 sensor (ExplorIR-M5%,CO2METER) to measure CO_2 molar composition. For homogenous mixing, the diaphragm pump and magnetic stirrers (Intllab) are used. To protect the CO_2 and flow sensors from the moisture in the outlet gas line, a drying tube (W A Hammond Drierite Co., LTD) is placed downstream of the bismuth reservoir. Voltage measurements are taken using the potentiostat measuring from two different electrode pairs, giving the cell voltage and two half-cell voltage readings. Image of the setup, experimental procedure and additional information is available in the supplementary information (See Supplementary Section 4.1)

Bismuth capacity utilization. Calculates percentage of the charge used by bismuth for acidification based on the experimental charge used to reach the minimum pH obtained from the filtered pH data during acidification, and the minimum charge required to reach that pH value, determined using the thermodynamic model. From this, the bismuth capacity utilization is calculated as:

$$Bismuth\ capacity\ utilization\ = \frac{Charge_{theoretical}}{Charge_{experimental}} * 100 \tag{18}$$

CO_2 flowrate. The downstream CO_2 molar flowrate is calculated using the known N_2 carrier-gas flowrate of 30 sccm. Assuming ideal-gas behavior and using 22.4 L mol^{-1} at standard temperature and pressure, this corresponds to an N_2 molar flowrate of 0.08 mol/hr. Given the measured CO_2 molar fraction (x_{CO_2}) from the sensor, the CO_2 molar flowrate is obtained from:

$$CO_2\ molar\ flowrate = \frac{0.08}{(1 - x_{CO2})} - 0.08 \tag{19}$$

Integrating the CO_2 molar flowrate above the baseline over time yields the total moles of CO_2 released and detected by the sensor (n_{CO_2}).

Lithium ICP measurements. During H-cell or flow cell experiments, samples are taken before and after each recovery using mechanical pipettes (Eppendorf). The volume drawn is based on the lithium concentration in the undilute solution, dilution factor (D.I) and the Inductively Coupled Plasma Mass Spectrometer (Thermo Scientific iCAP Qc at 4D-Labs) detection range in parts per billion (ppb). Samples are diluted using 2% HNO_3 up to total volume of 10 ml. The change in lithium composition in moles (Δn_{Li}) is calculated based on the recovery solution as:

$$\Delta n_{Li} = \left(V_{bulk,after} * Diluted_{ppb,after} - V_{bulk,before} * Diluted_{before}\right) * \frac{D.I}{10^6 * Mw_{Li}} \tag{20}$$

Lithium capacity utilization. Calculates the percentage of the charge used for lithium extraction over other cations, based on the change in lithium composition in the recovery solution in moles, Faraday's constant (96485 C/mol of e$^-$) and the experimental charge transferred. The equation used is:

$$Lithium\ capacity\ utilization = \frac{\Delta n_{Li} * 96485}{Charge_{experimental}} \tag{21}$$

View Article Online
DOI: 10.1039/D6TA03239G

Energy calculations. The energy consumed per mole of product (kJ/mol) is calculated from the net electrochemical cell energy of the extraction/acidification and recovery/alkalization phases, obtained from the area under the voltage-charge curve, and normalized by the moles of product produced. For the CO_2 detected, refer to equation 19. For the CO_2 released from thermodynamics, 90% of the aqueous CO_2 available for capture, based on the experiment's lowest pH during acidification, is used. For the extracted lithium ions, refer to equation 20. The energy consumption is calculated as:

$$Energy\ per\ mol\ of\ CO_2\ detected = \frac{Energy_{extraction} + Energy_{recovery}}{1000 * n_{CO_2,detected}} \quad (22)$$

$$Energy\ per\ mol\ of\ CO_2\ thermo = \frac{Energy_{extraction} + Energy_{recovery}}{1000 * n_{CO_2,thermo} * 0.90} \quad (23)$$

$$Energy\ per\ mol\ of\ Li = \frac{Energy_{extraction} + Energy_{recovery}}{1000 * \Delta n_{Li}} \quad (24)$$

Data Availability

The data supporting the findings of this study, including all experimental procedures, device schematics, and processed data presented in the figures, are provided in the Supplementary Information. Raw experimental data generated during this study will be deposited in a publicly accessible online repository (e.g., Zenodo) and made available upon publication of the article.

Author contributions

K.A. conceived the idea. S.A.H. and O.S. developed the thermodynamic model. O.S. designed experiments and performed the cell cycling experiments. K.A and O.S. analyzed the data and produced the final figures. K.A. and O.S. wrote the manuscript. S.A.H commented on the manuscript draft.

Competing interests

The authors declare no competing interests.

Acknowledgement

This work was supported by the Natural Sciences and Engineering Research Council of Canada (NSERC) Discovery Grant RGPIN-2024-03983 and Net-Zero for Materials and Manufacturing (Net0MM). We gratefully acknowledge the assistance and support of Jayson Garcia, Michael Nitzsche, Fabian Dickhardt, Li Tao, Dr. Aylin Aghababaei, Dr. Xin Zhang, Prof. Alexandra Tavasoli and Prof. Jian Liu.

Supplemental Information
Supplemental information is provided with this submission.

References

[1] K. Anderson, G. Peters, The trouble with negative emissions, Science (1979). 354 (2016) 182–183. https://doi.org/10.1126/science.aah4567.

[2] S. Kim, M.P. Nitzsche, S.B. Rufer, J.R. Lake, K.K. Varanasi, T.A. Hatton, Asymmetric chloride-mediated electrochemical process for CO2 removal from oceanwater, Energy Environ. Sci. (2023). https://doi.org/10.1039/d2ee03804h.

[3] M.D. Eisaman, K. Parajuly, A. Tuganov, C. Eldershaw, N. Chang, K.A. Littau, CO2 extraction from seawater using bipolar membrane electrodialysis, Energy Environ. Sci. 5 (2012) 7346–7352. https://doi.org/10.1039/C2EE03393C.

View Article Online
DOI: 10.1039/D6TA03239G

[4] L. Yan, J. Bao, Y. Shao, W. Wang, An Electrochemical Hydrogen-Looping System for Low-Cost CO2 Capture from Seawater, ACS Energy Lett. 7 (2022) 1947–1952. https://doi.org/https://pubs.acs.org/doi/10.1021/acsenergylett.2c00396.

[5] I.A. Digdaya, I. Sullivan, M. Lin, L. Han, W.H. Cheng, H.A. Atwater, C. Xiang, A direct coupled electrochemical system for capture and conversion of CO2 from oceanwater, Nature Communications 2020 11:1 11 (2020) 1–10. https://doi.org/10.1038/s41467-020-18232-y.

[6] P. Aleta, A. Refaie, M. Afshari, A. Hassan, M. Rahimi, Direct ocean capture: the emergence of electrochemical processes for oceanic carbon removal, Energy Environ. Sci. 16 (2023) 4944–4967. https://doi.org/10.1039/D3EE01471A.

[7] F.J. Millero, The marine inorganic carbon cycle, Chem. Rev. 107 (2007) 308–341. https://doi.org/https://doi.org/10.1021/cr0503557.

[8] C. Grosjean, P. Herrera Miranda, M. Perrin, P. Poggi, Assessment of world lithium resources and consequences of their geographic distribution on the expected development of the electric vehicle industry, Renewable and Sustainable Energy Reviews 16 (2012) 1735–1744. https://doi.org/10.1016/J.RSER.2011.11.023.

[9] A. Khalil, S. Mohammed, R. Hashaikeh, N. Hilal, Lithium recovery from brine: Recent developments and challenges, Desalination 528 (2022) 115611. https://doi.org/https://doi.org/10.1016/j.desal.2022.115611.

[10] Y. Zhang, W. Sun, R. Xu, L. Wang, H. Tang, Lithium extraction from water lithium resources through green electrochemical-battery approaches: A comprehensive review, J. Clean. Prod. 285 (2021) 124905. https://doi.org/10.1016/J.JCLEPRO.2020.124905.

[11] J. Wang, X. Yue, P. Wang, T. Yu, X. Du, X. Hao, A. Abudula, G. Guan, Electrochemical technologies for lithium recovery from liquid resources: A review, Renewable and Sustainable Energy Reviews 154 (2022) 111813. https://doi.org/10.1016/J.RSER.2021.111813.

[12] C. Liu, Y. Li, D. Lin, P.C. Hsu, B. Liu, G. Yan, T. Wu, Y. Cui, S. Chu, Lithium Extraction from Seawater through Pulsed Electrochemical Intercalation, Joule 4 (2020) 1459–1469. https://doi.org/10.1016/j.joule.2020.05.017.

[13] L. He, W. Xu, Y. Song, Y. Luo, X. Liu, Z. Zhao, New Insights into the Application of Lithium-Ion Battery Materials: Selective Extraction of Lithium from Brines via a Rocking-Chair Lithium-Ion Battery System, Global Challenges 2 (2018). https://doi.org/10.1002/gch2.201700079.

[14] G. Luo, X. Li, L. Chen, Y. Chao, W. Zhu, Electrochemical lithium ion pumps for lithium recovery: A systematic review and influencing factors analysis, Desalination 548 (2023) 116228. https://doi.org/10.1016/J.DESAL.2022.116228.

[15] A. Battistel, M.S. Palagonia, D. Brogioli, F. La Mantia, R. Trócoli, Electrochemical Methods for Lithium Recovery: A Comprehensive and Critical Review, Advanced Materials 32 (2020) 1905440. https://doi.org/10.1002/ADMA.201905440.

[16] X. Zhao, H. Yang, Y. Wang, Z. Sha, Review on the electrochemical extraction of lithium from seawater/brine, Journal of Electroanalytical Chemistry 850 (2019) 113389. https://doi.org/10.1016/J.JELECHEM.2019.113389.

[17] A. Ozden, CO2 Capture via Electrochemical pH-Mediated Systems, ACS Energy Lett. 20 (2025) 1550–1576. https://doi.org/https://doi.org/10.1021/acsenergylett.5c00200.

[18] J.C. Bui, É. Lucas, E.W. Lees, A.K. Liu, H.A. Atwater, C. Xiang, A.T. Bell, A.Z. Weber, Analysis of bipolar membranes for electrochemical CO2 capture from air and oceanwater, Energy Environ. Sci. 16 (2023) 5076–5095. https://doi.org/10.1039/D3EE01606D.

View Article Online
DOI: 10.1039/D6TA03239G

[19] Z.J. Schiffer, É. Lucas, N.B. Watkins, S. Ardo, C. Xiang, H.A. Atwater, Acid and base generation via an electrochemical hydrogen-looping cell tailored for carbon removal applications, Device 2 (2024) 100506. https://doi.org/10.1016/J.DEVICE.2024.100506.

[20] G.H. Rau, Electrochemical CO2 capture and storage with hydrogen generation, Energy Procedia 1 (2009) 823–828. https://doi.org/10.1016/J.EGYPRO.2009.01.109.

[21] F. Ali, D. Bilger, E.D. Patamia, T.L. Andrew, D.G. Kwabi, Towards Immobilized Proton-Coupled Electron Transfer Agents for Electrochemical Carbon Capture from Air and Seawater, J. Electrochem. Soc. 171 (2024) 053505. https://doi.org/10.1149/1945-7111/AD4A0F.

[22] M.E.Q. Pilson, An Introduction to the Chemistry of the Sea , Cambridge University Press, 2012.

[23] S.L. Clegg, M.P. Humphreys, J.F. Waters, D.R. Turner, A.G. Dickson, Chemical speciation models based upon the Pitzer activity coefficient equations, including the propagation of uncertainties. II. Tris buffers in artificial seawater at 25 °C, and an assessment of the seawater 'Total' pH scale, Mar. Chem. 244 (2022) 104096. https://doi.org/https://doi.org/10.1016/j.marchem.2022.104096.

[24] F.J. Millero, The estimation of the pK∗HA of acids in seawater using the Pitzer equations, Geochim. Cosmochim. Acta 47 (1983) 2121–2129. https://doi.org/10.1016/0016-7037(83)90037-6.

[25] F. Millero, D.S.-A.J. of Science, undefined 1982, Use of the ion pairing model to estimate activity coefficients of the ionic components of natural waters, Ajsonline.Org (n.d.). https://ajsonline.org/article/60252.pdf (accessed June 25, 2025).

[26] D.-H. Nam, K.-S. Choi, Bismuth as a New Chloride-Storage Electrode Enabling the Construction of a Practical High Capacity Desalination Battery, (2017). https://doi.org/10.1021/jacs.7b01119.

[27] J. Xiong, L. He, Z. Zhao, Lithium extraction from high-sodium raw brine with Li0.3FePO4 electrode, Desalination 535 (2022) 115822. https://doi.org/10.1016/J.DESAL.2022.115822.

[28] X. Yue, J. Wang, H. Zhou, C. Guo, J. Chen, X. Cai, F. Gong, X. Wang, Y. Lv, D. Huang, L. Wang, Reviving LiFePO4 electrode for long-term natural brine lithium extraction: mechanisms of impurity-ion induced attenuation and redox-mediated in-situ revitalization strategy, Water Res. 289 (2026) 124831. https://doi.org/10.1016/J.WATRES.2025.124831.

[29] C. Liu, P.C. Hsu, J. Xie, J. Zhao, T. Wu, H. Wang, W. Liu, J. Zhang, S. Chu, Y. Cui, A half-wave rectified alternating current electrochemical method for uranium extraction from seawater, Nature Energy 2017 2:4 2 (2017) 17007-. https://doi.org/10.1038/nenergy.2017.7.

[30] Z. Li, C. Li, X. Liu, L. Cao, P. Li, R. Wei, X. Li, D. Guo, K.-W. Huang, Z. Lai, Continuous electrical pumping membrane process for seawater lithium mining †, This Journal Is Cite This: Energy Environ. Sci 14 (2021) 3152. https://doi.org/10.1039/d1ee00354b.

[31] J. Yang, Y. Wang, M. Zhang, P. Wang, X. He, H. Zhou, P. He, Lithium Metal Recovery from Sea Water by a Flexible and Scalable Membrane with Lithium-Ion Exclusive Channels, Angew. Chem. Int. Ed. 63 (2024) e202411957. https://doi.org/https://doi.org/10.1002/anie.202411957.

[32] S. Kim, H. Joo, T. Moon, S.H. Kim, J. Yoon, Rapid and selective lithium recovery from desalination brine using an electrochemical system, Environ. Sci. Process. Impacts 21 (2019) 667–676. https://doi.org/10.1039/C8EM00498F.

[33] L. Kong, G. Yan, K. Hu, Y. Yu, N. Conte, K.R. Mckenzie, M.J. Wagner, S.G. Boyes, H. Chen, C. Liu, X. Liu, Electro-driven direct lithium extraction from geothermal brines to generate battery-grade lithium hydroxide, Nature Communications 2025 16:1 16 (2025) 806-. https://doi.org/10.1038/s41467-025-56071-x.

View Article Online
DOI: 10.1039/D6TA03239G

[34] Z. Li, I.C. Chen, L. Cao, X. Liu, K.W. Huang, Z. Lai, Lithium extraction from brine through a decoupled and membrane-free electrochemical cell design, Science (1979). 385 (2024) 1438–1444. https://doi.org/DOI:10.1126/science.adg8487.

[35] J. Yu, D. Fang, H. Zhang, Z.Y. Leong, J. Zhang, X. Li, H.Y. Yang, Ocean Mining: A Fluidic Electrochemical Route for Lithium Extraction from Seawater, ACS Mater. Lett. 2 (2020) 1662–1668. https://doi.org/https://doi.org/10.1021/acsmaterialslett.0c00385.

View Article Online
DOI: 10.1039/D6TA03239G

Data Availability

The data supporting the findings of this study, including all experimental procedures, device schematics, and processed data presented in the figures, are provided in the Supplementary Information. Raw experimental data generated during this study will be deposited in a publicly accessible online repository (e.g., Zenodo) and made available upon publication of the article.